International Journal of Mass Spectrometry 275 (2008) 21–33

Contents lists available at ScienceDirect

International Journal of Mass Spectrometry

journal homepage: www.elsevier.com/locate/ijms

Theory of the elliptical Penning trap

Martin Kretzschmar*

Institut für Physik, Johannes-Gutenberg-Universität, Staudinger-Weg 7, 55099 Mainz, Germany

ARTICLE INFO

Article history:
Received 5 March 2008
Received in revised form 5 May 2008
Accepted 5 May 2008
Available online 16 May 2008

PACS:
07.75.+h
21.10.Dr
32.10.Bi
82.80.Qx

Keywords:
Penning trap
Ion motion
Ion storage
Mass spectrometry
Frequency shift

ABSTRACT

An ideal "Elliptical Penning Trap" is an ideal cylindrically symmetric Penning trap with an additional electrostatic quadrupolar potential $\propto \kappa(x^2 - y^2)$. This configuration is here investigated for arbitrary strength κ of the additional potential. Aside from the decoupled axial motion the system is characterized by a generalized cyclotron and a generalized magnetron frequency. While the former depends only weakly on κ, the magnetron frequency decreases rapidly with increasing κ, vanishing at a maximum value κ_{max} which represents the stability limit for the magnetron motion. Magnetron orbits are elliptical, with their numerical excentricity tending toward unity as κ approaches its maximum value. A complete and rigorous description of the dynamics of the ideal elliptical trap is given, its approximate physical realization by use of a segmented ring electrode is discussed, and the frequency shifts expected for a real elliptical trap on account of anharmonic potential terms and of image charges are estimated by means of classical canonical perturbation theory. The accompanying paper by Breitenfeldt et al. [M. Breitenfeldt, S. Baruah, K. Blaum, A. Herlert, M. Kretzschmar, F. Martinez, G. Marx, L. Schweikhard, N. Walsh, Int. J. Mass Spectrom. (2008) this issue] reports corresponding experimental investigations.

1. Introduction

In recent years Penning traps have developed into valuable tools for high-precision measurements on electrons, atoms, molecules, clusters, and antiparticles [1–4]. The experimental goals of these investigations require a thorough understanding of the ion motion inside the trap and ever more refined methods for manipulating the ions. It is thus of interest to explore a variety of modifications of standard trap design and operation in search of advantageous new experimental techniques. With this motivation we have investigated here "elliptical" Penning traps, because they permit the control of the magnetron frequency and the shape of the magnetron orbit. Experimental results are presented in the accompanying paper by Breitenfeldt et al. [5].

The electromagnetic field configuration of a conventional Penning trap consists of a homogeneous magnetic field in z-direction (axial direction) and an electrostatic field $\propto (2z^2 - x^2 - y^2)$, produced by electrodes shaped as hyperboloids of revolution [1]. When an additional static quadrupolar field $\propto \kappa(x^2 - y^2)$ is present, for example due to imperfections of the trap, it has hitherto been viewed as an undesirable perturbation, and methods to correct for it have been developed [6–8]. Contrary to this view, we consider here the static quadrupolar field $\propto \kappa(x^2 - y^2)$ as an additional degree of freedom in the operation of the trap and explore the new opportunities resulting from the variation of the strength parameter κ. (For its precise definition see Eq. (14) below.) We present in this paper a complete and rigorous analysis of this linear system in the framework of Hamiltonian dynamics. As expected the system is described in terms of two frequencies, a generalized cyclotron frequency $\tilde{\omega}_+$ and a generalized magnetron frequency $\tilde{\omega}_-$. Under the usual operating conditions for a Penning trap the generalized cyclotron frequency changes only little with increasing κ, however, the generalized magnetron frequency $\tilde{\omega}_-$ decreases rapidly, while the magnetron orbit becomes elliptic with increasing numerical excentricity. For some maximum value κ_{max} one reaches a region of instability. At the limit point we find $\tilde{\omega}_- = 0$, and the magnetron orbit has degenerated into a straight line.

Elliptical Penning traps offering the possibility of varying the κ-parameter can be approximately realized in the laboratory by using a ring electrode (one-sheeted hyperboloid) divided into four or even eight sectors. Traps with this design are in use in many laboratories because they permit the introduction of rf-fields into the trap for the purpose of exciting the motional modes of the stored particles or of stimulating the interconversion of these modes [9,4]. The static electric potentials applied to the segments of the ring

* Tel.: +49 6131 477234.
E-mail address: Martin.Kretzschmar@uni-mainz.de.

1387-3806/$ – see front matter © 2008 Elsevier B.V. All rights reserved.
doi:10.1016/j.ijms.2008.05.009

electrode generate the quadrupolar field $\propto \kappa(x^2 - y^2)$ that makes the trap "elliptic" but this is one component among others, which represent higher multipole fields with anharmonic contributions to the static electric potential. Their influence must be minimized by an appropriate choice of the voltages applied to the various sectors of the ring electrode.

The paper is organized into two main chapters. The first one discusses the ion motion in an "ideal elliptical Penning trap" which is described by a Hamiltonian quadratic in the canonical coordinates q_i, p_i. This problem can be completely and rigorously solved. Ion trajectories in Cartesian coordinates are presented at the end of this chapter, the elliptical orbits are discussed in their dependence on the strength parameter κ. The second chapter treats a standard trap with a ring electrode divided into four or more segments and discusses to which extent the ideal elliptical Penning trap can be approximated by this configuration. This study uses Fourier analysis and perturbation theoretical methods as its tools.

2. The ideal elliptical Penning trap

2.1. The ideal Penning trap with axial rotational symmetry

In the ideal Penning trap with cylindrical symmetry [1] a particle of mass m and electric charge q is moving in a superposition of a homogeneous magnetic field $\vec{B}_0 = B_0\vec{e}_z$ in axial direction and a static electric field $\vec{E} = -\nabla\Phi_0(x, y, z)$ with the potential

$$\Phi_0 = \frac{U_0}{2z_0^2 + r_0^2}(2z^2 - x^2 - y^2). \tag{1}$$

The latter can be generated by two conducting surfaces (equipotential surfaces) shaped as hyperboloids of revolution, namely the one-sheeted "ring electrode" $2z^2 - x^2 - y^2 = -r_0^2$ and the two-sheeted "end electrodes" $2z^2 - x^2 - y^2 = 2z_0^2$, with a potential difference U_0 between ring and end electrodes. If $qU_0 > 0$ the particle oscillates in the z-direction with the "axial frequency" $\nu_z = \omega_z/(2\pi)$, where

$$\omega_z = \sqrt{\frac{4qU_0}{m(2z_0^2 + r_0^2)}}. \tag{2}$$

The two other degrees of freedom are circular motions (denoted as "azimuthal modes" or as "radial modes"), the "modified cyclotron motion" with frequency $\nu_+ = \omega_+/(2\pi)$ and the "magnetron drift" with frequency $\nu_- = \omega_-/(2\pi)$.

$$\omega_+ = \frac{1}{2}(\omega_c + \omega_1) \quad \text{(modified cyclotron frequency)}, \tag{3}$$

$$\omega_- = \frac{1}{2}(\omega_c - \omega_1) \quad \text{(magnetron frequency)}, \tag{4}$$

where $\omega_c = qB_0/m$ is the "true cyclotron frequency" and ω_1 is given by $\omega_1 = \sqrt{\omega_c^2 - 2\omega_z^2}$.

The Hamiltonian for ion motion in the ideal Penning trap is in Cartesian coordinates [10]

$$H_0 = \frac{1}{2m}(p_x^2 + p_y^2 + p_z^2) - \frac{1}{2}\omega_c(xp_y - yp_x) - \frac{m}{2}\left(\frac{\omega_1}{2}\right)^2(x^2 + y^2 - 2z^2). \tag{5}$$

The axial motion is independent of the other motional modes and can be separated, and the azimuthal motional modes can be decoupled by the canonical transformation

$$q_+ = \frac{1}{\sqrt{2}}\left(+\sqrt{\frac{m\omega_1}{2}}x - \sqrt{\frac{2}{m\omega_1}}p_y\right), \tag{6}$$

$$q_- = \frac{1}{\sqrt{2}}\left(+\sqrt{\frac{m\omega_1}{2}}x + \sqrt{\frac{2}{m\omega_1}}p_y\right), \tag{7}$$

$$p_+ = \frac{1}{\sqrt{2}}\left(+\sqrt{\frac{m\omega_1}{2}}y + \sqrt{\frac{2}{m\omega_1}}p_x\right), \tag{8}$$

$$p_- = \frac{1}{\sqrt{2}}\left(-\sqrt{\frac{m\omega_1}{2}}y + \sqrt{\frac{2}{m\omega_1}}p_x\right). \tag{9}$$

In these coordinates the transformed Hamiltonian of the ideal trap is given by

$$H_0 = \frac{\omega_+}{2}(q_+^2 + p_+^2) - \frac{\omega_-}{2}(q_-^2 + p_-^2). \tag{10}$$

2.2. The ideal elliptical Penning trap

In this paper we study an ideal cylindrically symmetric Penning trap (when restricted to the plane $z = 0$ it might be called a "circular" Penning trap) modified by an additional static quadrupolar potential $\propto x^2 - y^2$ with arbitrary strength. As discussed in more detail in Section 3 this modification can be approximately realized by a ring electrode divided into four or eight segments. In the ideal elliptical Penning trap an ion by definition has the total potential energy

$$V(x, y, z) = \frac{1}{4}m\omega_z^2(2z^2 - x^2 - y^2) + \frac{1}{4}m\omega_z^2\epsilon(x^2 - y^2), \tag{11}$$

where the "ellipticity parameter" ϵ measures the strength of the additional term. With the new term the axial motion still separates from the azimuthal cyclotron and magnetron motions. Therefore the axial mode will not be considered any further and we may restrict the following considerations to a particle moving in the plane $z = 0$. Thus from now on we work with the potential

$$V(x, y, z)|_{z=0} = -\frac{1}{4}m\omega_z^2((1 - \epsilon)x^2 + (1 + \epsilon)y^2). \tag{12}$$

This potential can be visualized as a surface which is

- for $\epsilon = 0$ a spherical hill top with circular equipotential lines;
- for $0 < |\epsilon| < 1$ a more or less elongated ridge with elliptical equipotential lines;
- for $|\epsilon| > 1$ a surface with hyperbolic equipotential lines and a saddle point at the trap center.

A charged particle moving in perpendicular *uniform* and static electric and magnetic fields experiences a drift in the direction of $\vec{E} \times \vec{B}$ ([11], p. 582). Therefore, we may expect for our problem that the magnetron drift of the cyclotron motion follows to a very good approximation the equipotential lines of the surface (12). For ellipticity values $0 < |\epsilon| < 1$ these are ellipses

$$\frac{x^2}{\left(R/\sqrt{1 - \epsilon}\right)^2} + \frac{y^2}{\left(R/\sqrt{1 + \epsilon}\right)^2} = 1, \tag{13}$$

with $a = R/\sqrt{1 - |\epsilon|}$ as major semi-axis and $b = R/\sqrt{1 + |\epsilon|}$ as minor semi-axis. For $\epsilon > 0$ the major (minor) semi-axis is parallel to the x-axis (y-axis), for $\epsilon < 0$ the major (minor) semi-axis is parallel to the y-axis (x-axis). On the other hand, for $|\epsilon| > 1$ we have unbounded hyperbolic orbits, so that in this case there is no trapping, magnetron motion lets the ions drift into infinity.

2.3. Hamiltonian description

For the discussion in the framework of Hamiltonian mechanics we must express the additional quadrupolar potential in terms of the canonical coordinates q_+, p_+, q_-, and p_-

$$H_1 = \frac{\epsilon\omega_z^2}{4\omega_1}(q_+ + q_-)^2 - \frac{\epsilon\omega_z^2}{4\omega_1}(p_+ - p_-)^2 = \frac{\kappa}{2}(q_+ + q_-)^2 - \frac{\kappa}{2}(p_+ - p_-)^2, \quad (14)$$

where for convenience of notation we have introduced the strength parameter $\kappa = \epsilon\omega_z^2/(2\omega_1)$. As shown in more detail below, at the ellipticity $\epsilon = \pm 1$ the magnetron motion changes its character from elliptic to hyperbolic, correspondingly for the operation of an elliptic Penning trap the strength parameter κ is limited to the range $0 \le |\kappa| < \kappa_{\max} = \omega_z^2/(2\omega_1) = \omega_+\omega_-/\omega_1$. The total Hamiltonian is obtained by addition of Eqs. (10) and (14)

$$H = H_0 + H_1. \quad (15)$$

2.3.1. The equations of motion and the eigenfrequencies

The equations of motion for the canonical coordinates of the cyclotron and magnetron modes are $\dot{q}_i = \partial H/\partial p_i$ and $\dot{p}_i = -\partial H/\partial q_i$, explicitly

$$\frac{\mathrm{d}}{\mathrm{d}t}\begin{pmatrix} q_+ \\ q_- \\ p_+ \\ p_- \end{pmatrix} = M \begin{pmatrix} q_+ \\ q_- \\ p_+ \\ p_- \end{pmatrix} \quad (16)$$

with

$$M = \begin{pmatrix} 0 & 0 & \omega_+ - \kappa & \kappa \\ 0 & 0 & \kappa & -(\omega_- + \kappa) \\ -(\omega_+ + \kappa) & -\kappa & 0 & 0 \\ -\kappa & \omega_- - \kappa & 0 & 0 \end{pmatrix} \quad (17)$$

With $\omega_1 = \omega_+ - \omega_-$ the iteration of these equations yields

$$\frac{\mathrm{d}^2}{\mathrm{d}t^2}\begin{pmatrix} q_+ \\ q_- \\ p_+ \\ p_- \end{pmatrix} = -\begin{pmatrix} \omega_+^2 & \kappa\omega_1 & 0 & 0 \\ \kappa\omega_1 & \omega_-^2 & 0 & 0 \\ 0 & 0 & \omega_+^2 & \kappa\omega_1 \\ 0 & 0 & \kappa\omega_1 & \omega_-^2 \end{pmatrix} \begin{pmatrix} q_+ \\ q_- \\ p_+ \\ p_- \end{pmatrix}. \quad (18)$$

From the matrix of either of these equations the algebraic equation determining the eigenvalues of the system is obtained as

$$(\lambda^2 + \omega_+^2)(\lambda^2 + \omega_-^2) - \kappa^2\omega_1^2 = 0. \quad (19)$$

The four roots of this equation can be expressed as $\lambda_{1,2} = \pm i\tilde{\omega}_+$ and $\lambda_{3,4} = \pm i\tilde{\omega}_-$, where $\tilde{\omega}_+$ and $\tilde{\omega}_-$ are the generalized cyclotron and magnetron frequencies. They are calculated as

$$\tilde{\omega}_+^2 = \omega_+^2 + \kappa\omega_1 \cdot K(\kappa), \quad (20)$$

$$\tilde{\omega}_-^2 = \omega_-^2 - \kappa\omega_1 \cdot K(\kappa). \quad (21)$$

On the right hand side we have introduced the convenient abbreviation

$$K(\kappa) = \frac{\omega_c}{2\kappa}\left[\sqrt{1 + \frac{4\kappa^2}{\omega_c^2}} - 1\right] = \frac{2\kappa}{\omega_c}\left[\sqrt{1 + \frac{4\kappa^2}{\omega_c^2}} + 1\right]^{-1}, \quad (22)$$

or in terms of the ellipticity parameter ϵ

$$K(\epsilon) = \frac{\epsilon\omega_z^2}{\omega_1\omega_c + \sqrt{\omega_1^2\omega_c^2 + \epsilon^2\omega_z^4}} = \frac{1}{\epsilon\omega_z^2}\left[\sqrt{\omega_1^2\omega_c^2 + \epsilon^2\omega_z^4} - \omega_1\omega_c\right]. \quad (23)$$

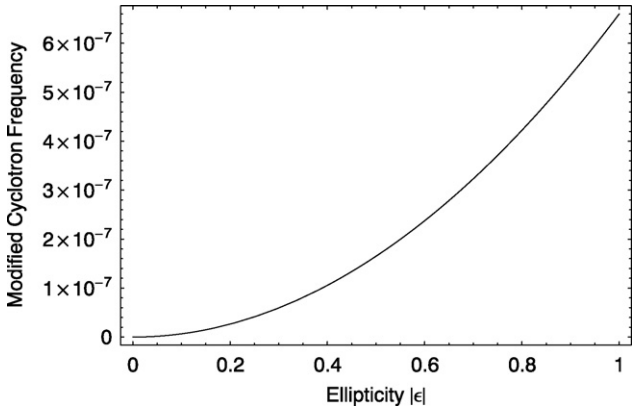

Fig. 1. Generalized cyclotron frequency $\tilde{\omega}_+$. The plot shows $(\tilde{\omega}_+ - \omega_+)/\omega_+$ as a function of the ellipticity $\epsilon = \kappa/\kappa_{\max}$. In the limit $\epsilon = 0$ we have $\tilde{\omega}_+ = \omega_+$, in the limit $\epsilon = 1$ we have $\tilde{\omega}_+ = \sqrt{\omega_c^2 - \omega_z^2}$.

An important consequence of the relations (20) and (21) is the general validity of the invariance theorem of Brown and Gabrielse [1], independently of the specific value of the ellipticity ϵ

$$\tilde{\omega}_+^2 + \tilde{\omega}_-^2 + \omega_z^2 = \omega_+^2 + \omega_-^2 + \omega_z^2 = \omega_c^2. \quad (24)$$

On the other hand, for nonvanishing ellipticity we observe $\tilde{\omega}_+ + \tilde{\omega}_- \neq \omega_c$ for $\epsilon \neq 0$.

The explicit expressions for the generalized cyclotron and magnetron frequencies as functions of the strength parameter κ and the ellipticity parameter ϵ, respectively, become

$$\tilde{\omega}_+ = \sqrt{\omega_+^2 + \kappa\omega_1 \cdot K(\kappa)} = \sqrt{\frac{1}{2}(\omega_c^2 - \omega_z^2) + \frac{1}{2}\sqrt{\omega_c^2\omega_1^2 + \epsilon^2\omega_z^4}} \quad (25)$$

$$\tilde{\omega}_- = \sqrt{\omega_-^2 - \kappa\omega_1 \cdot K(\kappa)} = \sqrt{\frac{1}{2}(\omega_c^2 - \omega_z^2) - \frac{1}{2}\sqrt{\omega_c^2\omega_1^2 + \epsilon^2\omega_z^4}} \quad (26)$$

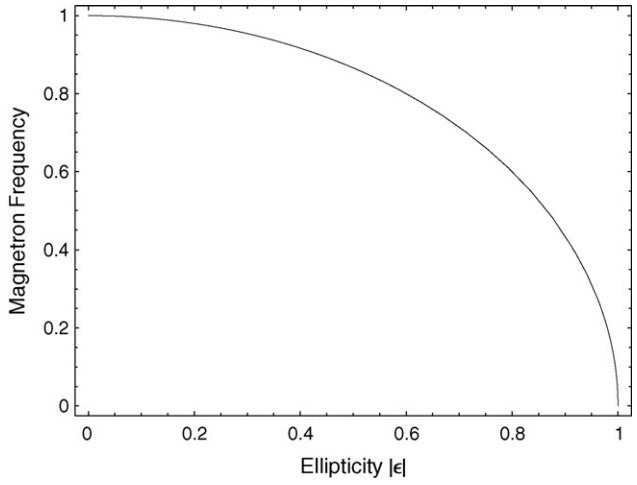

Fig. 2. Generalized magnetron frequency $\tilde{\omega}_-$. The plot shows $\tilde{\omega}_-/\omega_-$ as a function of the ellipticity $\epsilon = \kappa/\kappa_{\max}$. In the limit $\epsilon \to 0$ we have $\tilde{\omega}_- = \omega_-$, in the limit $\epsilon \to 1$ we have $\tilde{\omega}_- = 0$.

Figs. 1 and 2 display the typical dependence of these frequencies[1] on $|\epsilon|$: the generalized cyclotron frequency $\tilde{\omega}_+(\epsilon)$ is increasing from $\tilde{\omega}_+(0)=\omega_+$ to $\tilde{\omega}_+(1)=\sqrt{\omega_c^2-\omega_z^2}$. Expressed by means of the invariance theorem (24) this is $\tilde{\omega}_+^2(1)-\tilde{\omega}_+^2(0)=\omega_-^2$. Under typical operating conditions of the Penning trap the magnetron frequency is several orders of magnitude smaller than the cyclotron frequency, so that the increase of $\tilde{\omega}_+$ is in fact very small. On the other hand, the generalized magnetron frequency $\tilde{\omega}_-(\epsilon)$ is monotonically decreasing from $\tilde{\omega}_-(0)=\omega_-$ to $\tilde{\omega}_-(1)=0$. Thus for $\epsilon=1$ the magnetron frequency vanishes and becomes imaginary for $|\epsilon|>1$, indicating the transition from bounded elliptical to unbounded hyperbolic motion.

2.3.2. The generalized eigenmodes

The Hamiltonian Eq. (15) is a symmetric quadratic form in the canonical coordinates and momenta q_+, q_-, p_+, and p_-. General theorems tell us that there exists a linear canonical transformation to new coordinates and momenta $\tilde{q}_+$, $\tilde{q}_-$, $\tilde{p}_+$, and $\tilde{p}_-$

$$\begin{pmatrix} q_+ \\ q_- \\ p_+ \\ p_- \end{pmatrix} = \begin{pmatrix} a_{11} & a_{12} & a_{13} & a_{14} \\ a_{21} & a_{22} & a_{23} & a_{24} \\ a_{31} & a_{32} & a_{33} & a_{34} \\ a_{41} & a_{42} & a_{43} & a_{44} \end{pmatrix} \begin{pmatrix} \tilde{q}_+ \\ \tilde{q}_- \\ \tilde{p}_+ \\ \tilde{p}_- \end{pmatrix}, \tag{27}$$

such that the new Hamiltonian takes the form

$$H(\tilde{q},\tilde{p}) = \frac{\tilde{\omega}_+}{2}(\tilde{q}_+^2(t)+\tilde{p}_+^2(t)) - \frac{\tilde{\omega}_-}{2}(\tilde{q}_-^2(t)+\tilde{p}_-^2(t)), \tag{28}$$

where $\tilde{\omega}_+$ and $\tilde{\omega}_-$ are the eigenfrequencies that we have determined in the preceding subsection and the matrix $A=(a_{ik})$ is a symplectic matrix with determinant 1. The new equations of motion are

$$\frac{\mathrm{d}}{\mathrm{d}t}\tilde{q}_\pm(t) = \frac{\partial H}{\partial p_\pm} = \pm\tilde{\omega}_\pm\tilde{p}_\pm, \tag{29}$$

$$\frac{\mathrm{d}}{\mathrm{d}t}\tilde{p}_\pm(t) = -\frac{\partial H}{\partial q_\pm} = \mp\tilde{\omega}_\pm\tilde{q}_\pm. \tag{30}$$

Their general solution can be written in terms of the phase variables $\tilde{\varphi}_\pm=\tilde{\omega}_\pm t+\tilde{\chi}_\pm$ as

$$\tilde{q}_+(t) = \tilde{A}_+\cos\tilde{\varphi}_+(t), \tag{31}$$

$$\tilde{p}_+(t) = -\tilde{A}_+\sin\tilde{\varphi}_+(t), \tag{32}$$

$$\tilde{q}_-(t) = \tilde{A}_-\cos\tilde{\varphi}_-(t), \tag{33}$$

$$\tilde{p}_-(t) = \tilde{A}_-\sin\tilde{\varphi}_-(t). \tag{34}$$

This solution depends on four arbitrary constants, the two amplitudes $\tilde{A}_+$, $\tilde{A}_-$, and the two phases $\tilde{\chi}_+$ and $\tilde{\chi}_-$. It remains to determine explicitly the canonical transformation (27) that takes us from the canonical variables $q_\pm$, $p_\pm$ to the new variables $\tilde{q}_\pm$, $\tilde{p}_\pm$.

2.3.3. The canonical transformation to eigenmodes

From the block structure of the equations of motion, Eqs. (16)–(18), together with the general form of the eigenmodes, Eqs. (31)–(34), we can conclude that the matrix $A=(a_{ik})$ of the desired canonical transformation must possess a corresponding block structure, with nonvanishing elements in the diagonal blocks and zeroes in the nondiagonal blocks. After insertion of the general form of the eigenmodes, Eqs. (31)–(34), and their equations of motion, Eqs. (29)–(30), into Eq. (18) we can extract the following matrix equation for $A=(a_{ik})$

$$\begin{pmatrix} a_{11} & a_{12} & 0 & 0 \\ a_{21} & a_{22} & 0 & 0 \\ 0 & 0 & a_{33} & a_{34} \\ 0 & 0 & a_{43} & a_{44} \end{pmatrix} \begin{pmatrix} \tilde{\omega}_+^2 & 0 & 0 & 0 \\ 0 & \tilde{\omega}_-^2 & 0 & 0 \\ 0 & 0 & \tilde{\omega}_+^2 & 0 \\ 0 & 0 & 0 & \tilde{\omega}_-^2 \end{pmatrix}$$
$$= \begin{pmatrix} \omega_+^2 & \kappa\omega_1 & 0 & 0 \\ \kappa\omega_1 & \omega_-^2 & 0 & 0 \\ 0 & 0 & \omega_+^2 & \kappa\omega_1 \\ 0 & 0 & \kappa\omega_1 & \omega_-^2 \end{pmatrix} \begin{pmatrix} a_{11} & a_{12} & 0 & 0 \\ a_{21} & a_{22} & 0 & 0 \\ 0 & 0 & a_{33} & a_{34} \\ 0 & 0 & a_{43} & a_{44} \end{pmatrix}. \tag{35}$$

The comparison of the matrix elements on both sides makes use of the relations $\tilde{\omega}_\pm^2-\omega_\pm^2=\pm\kappa\omega_1\cdot K(\kappa)$ and $\tilde{\omega}_\pm^2-\omega_\mp^2=\pm\kappa\omega_1\cdot K(\kappa)\pm\omega_c\omega_1$ and yields the results

$$a_{12} = -K(\kappa)\cdot a_{22}, \qquad a_{34} = -K(\kappa)\cdot a_{44}, \tag{36}$$

$$a_{21} = +K(\kappa)\cdot a_{11}, \qquad a_{43} = +K(\kappa)\cdot a_{33}. \tag{37}$$

The matrix $A=(a_{ik})$ is unimodular and must tend to the unit matrix in the limit $\kappa\to 0$, thus we find the condition

$$\det A = a_{11}a_{22}a_{33}a_{44}\cdot(1+K^2(\kappa)) = 1. \tag{38}$$

Finally, the firstorder equations (16) must be exploited. They tell us

$$\begin{pmatrix} a_{11} & a_{12} & 0 & 0 \\ a_{21} & a_{22} & 0 & 0 \\ 0 & 0 & a_{33} & a_{34} \\ 0 & 0 & a_{43} & a_{44} \end{pmatrix} \begin{pmatrix} 0 & 0 & \tilde{\omega}_+ & 0 \\ 0 & 0 & 0 & -\tilde{\omega}_- \\ -\tilde{\omega}_+ & 0 & 0 & 0 \\ 0 & \tilde{\omega}_- & 0 & 0 \end{pmatrix}$$
$$= \begin{pmatrix} 0 & 0 & \omega_+-\kappa & \kappa \\ 0 & 0 & \kappa & -(\omega_-+\kappa) \\ -(\omega_++\kappa) & -\kappa & 0 & 0 \\ -\kappa & \omega_--\kappa & 0 & 0 \end{pmatrix}$$
$$\times \begin{pmatrix} a_{11} & a_{12} & 0 & 0 \\ a_{21} & a_{22} & 0 & 0 \\ 0 & 0 & a_{33} & a_{34} \\ 0 & 0 & a_{43} & a_{44} \end{pmatrix}. \tag{39}$$

Taking into account previous results we drive the conditions

$$\omega_+ + \kappa(K(\kappa)+1)\cdot a_{11} = \tilde{\omega}_+\cdot a_{33}, \tag{40}$$

$$\omega_+ + \kappa(K(\kappa)-1)\cdot a_{33} = \tilde{\omega}_+\cdot a_{11}, \tag{41}$$

$$\omega_- + \kappa(K(\kappa)+1)\cdot a_{44} = \tilde{\omega}_-\cdot a_{22}, \tag{42}$$

$$\omega_- + \kappa(K(\kappa)-1)\cdot a_{22} = \tilde{\omega}_-\cdot a_{44}. \tag{43}$$

In order to show that these relations are consistent and in order to give them a more symmetrical appearance we deduce from Eq. (22)

$$K^2(\kappa) = 1-(\omega_c/\kappa)K(\kappa) = 1-(2\omega_1\omega_c)/(\epsilon\omega_z^2)K(\epsilon). \tag{44}$$

Using this result one finds the following factorizations of $\tilde{\omega}_+^2$ and $\tilde{\omega}_-$:

$$\tilde{\omega}_+^2 = (\omega_+ + \kappa(K(\kappa)+1))\cdot(\omega_+ + \kappa(K(\kappa)-1)), \tag{45}$$

$$\tilde{\omega}_-^2 = (\omega_- + \kappa(K(\kappa)+1))\cdot(\omega_- + \kappa(K(\kappa)-1)). \tag{46}$$

With their help the Eqs. (40)–(43) can be written in the form

$$\sqrt{\frac{\omega_+ + \kappa(K(\kappa)-1)}{\tilde{\omega}_+}}\cdot a_{33} = \sqrt{\frac{\omega_+ + \kappa(K(\kappa)+1)}{\tilde{\omega}_+}}\cdot a_{11}, \tag{47}$$

$$\sqrt{\frac{\omega_- + \kappa(K(\kappa)-1)}{\tilde{\omega}_-}}\cdot a_{22} = \sqrt{\frac{\omega_- + \kappa(K(\kappa)+1)}{\tilde{\omega}_-}}\cdot a_{44}. \tag{48}$$

[1] This figure and all following ones have been computed with the parameters $\omega_c = 2\pi\cdot 919\,\mathrm{kHz}$ and $\omega_z = 2\pi\cdot 44\,\mathrm{kHz}$.

These relations together with the determinant condition Eq. (38) yield the diagonal elements of A,

$$a_{11} = \sqrt{\frac{\omega_+ + \kappa(K(\kappa)-1)}{\tilde{\omega}_+(1+K^2(\kappa))}}, \qquad a_{22} = \sqrt{\frac{\omega_- + \kappa(K(\kappa)+1)}{\tilde{\omega}_-(1+K^2(\kappa))}}, \tag{49}$$

$$a_{33} = \sqrt{\frac{\omega_+ + \kappa(K(\kappa)+1)}{\tilde{\omega}_+(1+K^2(\kappa))}}, \qquad a_{44} = \sqrt{\frac{\omega_- + \kappa(K(\kappa)-1)}{\tilde{\omega}_-(1+K^2(\kappa))}}. \tag{50}$$

For subsequent use we collect our results in the transformation equations

$$q_+(t) = \sqrt{\frac{\omega_+ + \kappa(K(\kappa)-1)}{\tilde{\omega}_+(1+K^2(\kappa))}} \cdot \tilde{q}_+(t) - \sqrt{\frac{\omega_- + \kappa(K(\kappa)+1)}{\tilde{\omega}_-(1+K^2(\kappa))}} \cdot K(\kappa) \cdot \tilde{q}_-(t), \tag{51}$$

$$q_-(t) = \sqrt{\frac{\omega_+ + \kappa(K(\kappa)-1)}{\tilde{\omega}_+(1+K^2(\kappa))}} \cdot K(\kappa) \cdot \tilde{q}_+(t) + \sqrt{\frac{\omega_- + \kappa(K(\kappa)+1)}{\tilde{\omega}_-(1+K^2(\kappa))}} \cdot \tilde{q}_-(t), \tag{52}$$

$$p_+(t) = \sqrt{\frac{\omega_+ + \kappa(K(\kappa)+1)}{\tilde{\omega}_+(1+K^2(\kappa))}} \cdot \tilde{p}_+(t) - \sqrt{\frac{\omega_- + \kappa(K(\kappa)-1)}{\tilde{\omega}_-(1+K^2(\kappa))}} \cdot K(\kappa) \cdot \tilde{p}_-(t), \tag{53}$$

$$p_-(t) = \sqrt{\frac{\omega_+ + \kappa(K(\kappa)+1)}{\tilde{\omega}_+(1+K^2(\kappa))}} \cdot K(\kappa) \cdot \tilde{p}_+(t) + \sqrt{\frac{\omega_- + \kappa(K(\kappa)-1)}{\tilde{\omega}_-(1+K^2(\kappa))}} \cdot \tilde{p}_-(t). \tag{54}$$

2.4. Ion trajectories in position space

In the preceding section we have rigorously solved the equations of motion of an ion in an elliptical Penning trap using abstract canonical coordinates $\tilde{q}_\pm$, $\tilde{p}_\pm$. To visualize the ion trajectories in ordinary space we must relate these coordinates to Cartesian coordinates x, y. We start by inverting Eqs. (6)–(9) to obtain

$$x(t) = \frac{1}{\sqrt{m\omega_1}}(q_+(t) + q_-(t)), \tag{55}$$

$$y(t) = \frac{1}{\sqrt{m\omega_1}}(p_+(t) - p_-(t)). \tag{56}$$

Here we insert our Eqs. (51)–(54), the general solution Eqs. (31)–(34), and express the constants $\tilde{A}_+$ and $\tilde{A}_-$ in terms of size parameters $\tilde{R}_+ = \tilde{A}_+/\sqrt{m\omega_1}$ and $\tilde{R}_- = \tilde{A}_-/\sqrt{m\omega_1}$. These have the physical dimension of a length and generalize the concepts of the cyclotron and magnetron radii. Thus, we find the ion orbits

$$x(t) = \frac{1}{\sqrt{m\omega_1}}\left(\xi_+\tilde{q}_+(t) + \xi_-\tilde{q}_-(t)\right) = \xi_+\tilde{R}_+\cos\tilde{\varphi}_+(t) + \xi_-\tilde{R}_-\cos\tilde{\varphi}_-(t), \tag{57}$$

$$y(t) = \frac{1}{\sqrt{m\omega_1}}(\eta_+\tilde{p}_+(t) - \eta_-\tilde{p}_-(t)) = -\left(\eta_+\tilde{R}_+\sin\tilde{\varphi}_+(t) + \eta_-\tilde{R}_-\sin\tilde{\varphi}_-(t)\right). \tag{58}$$

The ion motion obviously is a superposition of two elliptical motions with their axes in the x-direction and y-direction, a cyclotron motion with semi-axes $\xi_+\tilde{R}_+$ and $\eta_+\tilde{R}_+$, and a magnetron drift motion with semi-axes $\xi_-\tilde{R}_-$ and $\eta_-\tilde{R}_-$. A given ion trajectory can be specified by four numbers, the values of $\tilde{R}_+$, $\tilde{R}_-$, and of the two phases $\tilde{\varphi}_+$, $\tilde{\varphi}_-$ at some initial time t_0. The quantities ξ_+, η_+, ξ_-, and η_- are "normalized" semi-axes, in other words, they are the semi-axes of the "unit ellipses" defined by $\tilde{R}_+ = 1$ and $\tilde{R}_- = 1$. In the limit of vanishing ellipticity $\epsilon \to 0$ all normalized semi-axes tend to the value 1, so that in this limit the motions become circular. All dependence on ellipticity is contained in the normalized semi-axes and in the characteristic frequencies $\tilde{\omega}_+$ and $\tilde{\omega}_-$.

The calculation of the normalized semi-axes as a function of the ellipticity ϵ requires a certain amount of algebra. From Eq. (22) one deduces

$$\frac{(1 \pm K(\kappa))^2}{1+K^2(\kappa)} = \frac{\omega_c + 2\kappa(K(\kappa) \pm 1)}{\omega_c + 2\kappa K(\kappa)}, \tag{59}$$

and with the help of this relation one obtains the following expressions:

$$\xi_+ = \sqrt{\frac{\omega_+\omega_c + \kappa\omega_1(1+K)}{\tilde{\omega}_+(\omega_c + 2\kappa K)}} = \sqrt{\frac{\omega_c^2 + \epsilon\omega_z^2 + \sqrt{\omega_c^2\omega_1^2 + \epsilon^2\omega_z^4}}{(2\tilde{\omega}_+/\omega_1)\cdot\sqrt{\omega_c^2\omega_1^2 + \epsilon^2\omega_z^4}}}, \tag{60}$$

$$\eta_+ = \sqrt{\frac{\omega_+\omega_c - \kappa\omega_1(1-K)}{\tilde{\omega}_+(\omega_c + 2\kappa K)}} = \sqrt{\frac{\omega_c^2 - \epsilon\omega_z^2 + \sqrt{\omega_c^2\omega_1^2 + \epsilon^2\omega_z^4}}{(2\tilde{\omega}_+/\omega_1)\cdot\sqrt{\omega_c^2\omega_1^2 + \epsilon^2\omega_z^4}}}, \tag{61}$$

$$\xi_- = \sqrt{\frac{\omega_-\omega_c + \kappa\omega_1(1-K)}{\tilde{\omega}_-(\omega_c + 2\kappa K)}} = \sqrt{\frac{\omega_c^2 + \epsilon\omega_z^2 - \sqrt{\omega_c^2\omega_1^2 + \epsilon^2\omega_z^4}}{(2\tilde{\omega}_-/\omega_1)\cdot\sqrt{\omega_c^2\omega_1^2 + \epsilon^2\omega_z^4}}}, \tag{62}$$

$$\eta_- = \sqrt{\frac{\omega_-\omega_c - \kappa\omega_1(1+K)}{\tilde{\omega}_-(\omega_c + 2\kappa K)}} = \sqrt{\frac{\omega_c^2 - \epsilon\omega_z^2 - \sqrt{\omega_c^2\omega_1^2 + \epsilon^2\omega_z^4}}{(2\tilde{\omega}_-/\omega_1)\cdot\sqrt{\omega_c^2\omega_1^2 + \epsilon^2\omega_z^4}}}. \tag{63}$$

Inspection of these expressions shows that for $0 < \epsilon < 1$ the major semi-axes of the cyclotron and the magnetron ellipses point in x-direction, *i.e.*, they are given by ξ_+ and ξ_-. For $-1 < \epsilon < 0$ the major semi-axes point in y-direction and are given by η_+ and η_-. The normalized semi-axes have been plotted as functions of the ellipticity ϵ, both for cyclotron motion (Fig. 3) and for magnetron motion (Fig. 4). While the cyclotron orbit remains nearly circular for all values of ϵ, the magnetron orbit undergoes dramatic change as $\epsilon \to 1$, the major semi-axis tends to infinity, while the minor semi-axis tends to zero. This holds for the ideal elliptic trap, which is a spatially unlimited field configuration, in a real trap the ion would hit the ring electrode before reaching the limit $\epsilon = 1$.

The numerical excentricity of an ellipse with major semi-axis a and minor semi-axis b is defined as $\mathcal{E} = \sqrt{1 - b^2/a^2}$. Thus for the cyclotron and magnetron motions the preceding results imply

$$\mathcal{E}_+ = \sqrt{\frac{2|\kappa|\omega_1}{\omega_+\omega_c + |\kappa|\omega_1(1+K)}} = \sqrt{\frac{2|\epsilon|\omega_z^2}{\omega_c^2 + |\epsilon|\omega_z^2 + \sqrt{\omega_c^2\omega_1^2 + |\epsilon|^2\omega_z^4}}}, \tag{64}$$

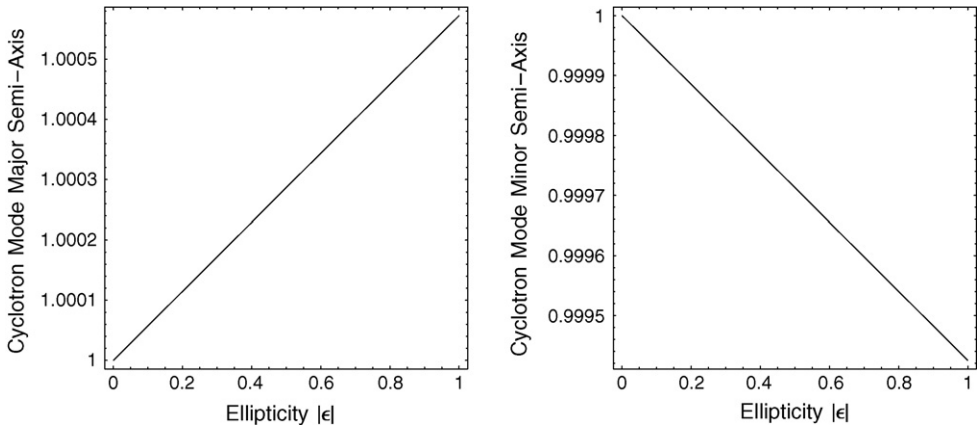

Fig. 3. Normalized major and minor semi-axes of the cyclotron orbit as a function of the ellipticity ϵ.

$$\mathcal{E}_- = \sqrt{\frac{2|\kappa|\omega_1}{\omega_-\omega_c + |\kappa|\omega_1(1-K)}} = \sqrt{\frac{2|\epsilon|\omega_z^2}{\omega_c^2 + |\epsilon|\omega_z^2 - \sqrt{\omega_c^2\omega_1^2 + |\epsilon|^2\omega_z^4}}}. \quad (65)$$

These excentricities are plotted in Fig. 5 as functions of the ellipticity ϵ. While $\mathcal{E}_+$ remains small over the whole range of ϵ, the excentricity of the magnetron orbit approaches the value 1 as $|\epsilon| \to 1$.

For $\epsilon = 0$ the magnetron drift velocity is constant in time and equals $v_-^0 = \omega_- R_-$. For $\epsilon \neq 0$, however, it varies along the magnetron orbit. From Eqs. (57) and (58) we obtain the velocity as

$$v_-(\tilde{\varphi}_-, \epsilon) = \tilde{\omega}_-(\epsilon)\tilde{\xi}_-(\epsilon)\tilde{R}_- \cdot \sqrt{1 - \mathcal{E}_-^2(\epsilon)\cos^2\tilde{\varphi}_-}, \quad (66)$$

where for definiteness we have assumed $\epsilon \geq 0$, so that the large semi-axis of the magnetron ellipse is $\tilde{\xi}_-\tilde{R}_-$. For $\epsilon < 0$ the roles of ξ_- and η_- are interchanged. For comparison to the case $\epsilon = 0$ we have studied the "normalized" drift velocity $v_-(\tilde{\varphi}_-, \epsilon)/(\omega_- R_-)$. Fig. 6 shows its maximum ($\tilde{\varphi}_- = \pi/2$) and minimum ($\tilde{\varphi}_- = 0$) values as a function of ϵ, while Fig. 7 plots the values of the normalized magnetron drift velocity as a function of the azimuthal angle $\tilde{\varphi}_-$.

3. The real elliptical Penning trap

How can the idealized field configuration analyzed in the preceding sections be practically realized in the laboratory? The obvious idea of manufacturing conducting metal electrodes with the shape of the equipotential surfaces $2z^2 - (1-\epsilon)x^2 - (1+\epsilon)y^2 = r_0^2$ (elliptical ring electrode) and $2z^2 - (1-\epsilon)x^2 - (1+\epsilon)y^2 = -z_0^2$ (elliptical endcap electrodes) is not very appealing, because the ellipticity parameter ϵ can not be varied. In practice one uses a Penning trap with a segmented ring electrode, by which one can introduce into the trap an additional electrostatic potential, the "elliptic" potential U_{ell}, chosen to approximate in the best possible way the interaction term Eq. (14) characteristic of the ideal elliptic Penning trap. Penning traps with ring electrodes divided into four or eight segments are in actual use in many laboratories [5] for various other reasons. To be more specific let us assume that the ring electrode is divided into N segments, the dividing slits being located at the angular coordinates $\varphi_1, \varphi_2, \ldots, \varphi_N = \varphi_0$, with each segment subtending an angular range $\Delta_i = \varphi_i - \varphi_{i-1}$ and carrying a static electric potential U_i, for $i = 1, \ldots, N$. The potentials are adjusted to produce the best possible approximation to the ideal elliptic Penning trap, however, anharmonic deviations are inevitably present, in addition to the usual imperfections.

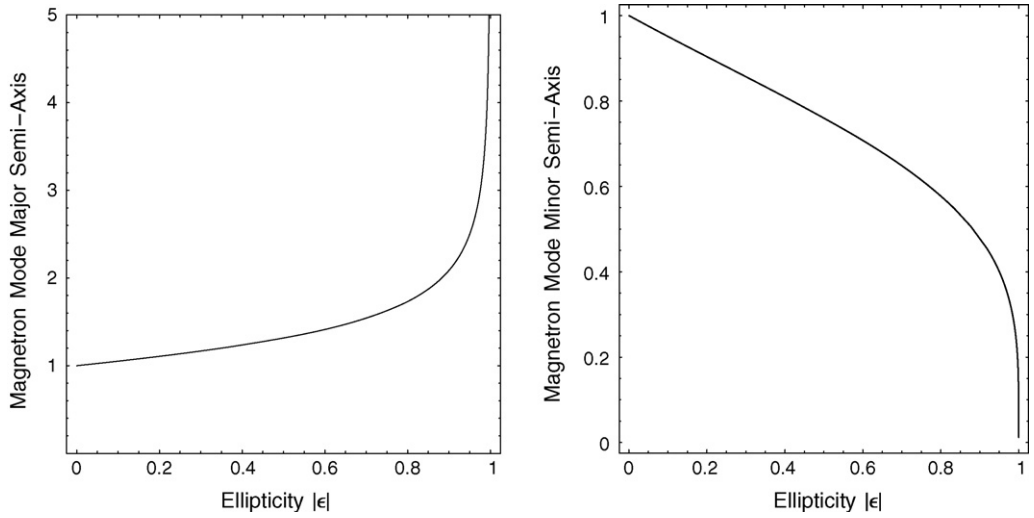

Fig. 4. Normalized major and minor semi-axes of the magnetron orbit as functions of the ellipticity ϵ.

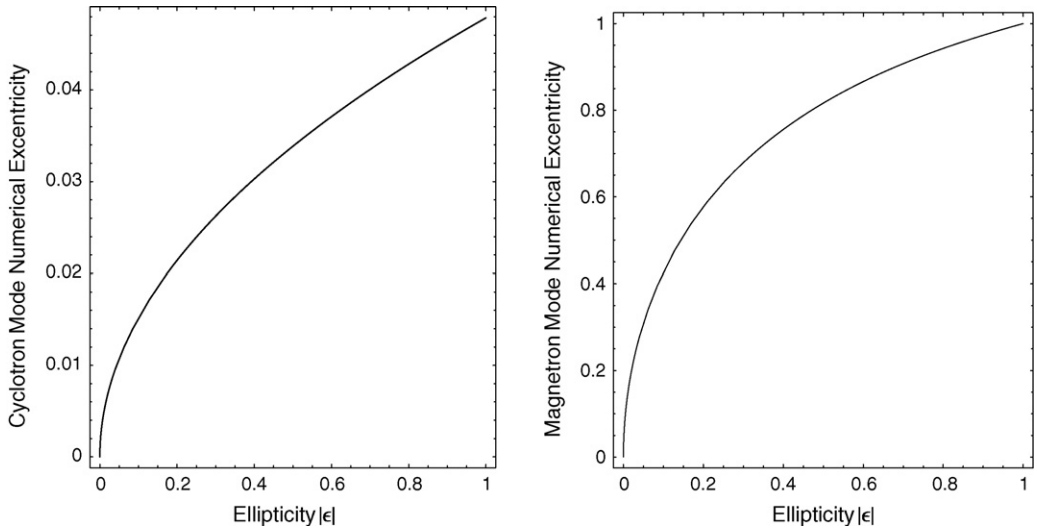

Fig. 5. Numerical excentricities $\mathcal{E}_+$ of the cyclotron orbit and $\mathcal{E}_-$ of the magnetron orbit as a function of the ellipticity $|\epsilon|$. Note the different scales on the two plots.

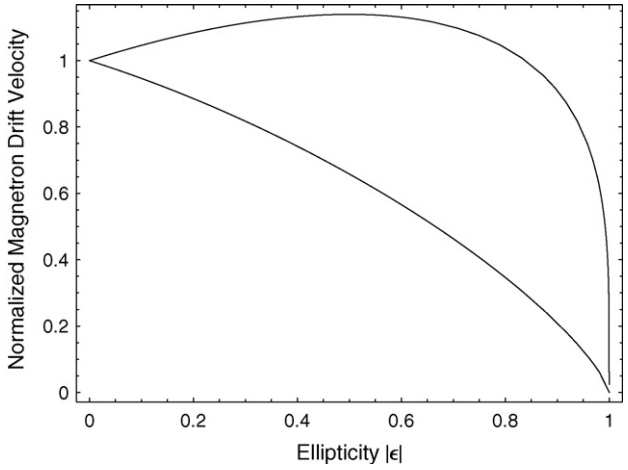

Fig. 6. Maximum and minimum values of the normalized magnetron drift velocity as a function of $|\epsilon|$.

3.1. Fourier analysis

Assuming $\Delta_1 = \Delta_5$, $\Delta_2 = \Delta_4 = \Delta_6 = \Delta_8$, and $\Delta_3 = \Delta_7$, and choosing the potentials as $U_1 = U_5$, $U_2 = U_4 = U_6 = U_8$, and $U_3 = U_7$, we obtain a potential $U_{\mathrm{ell}}(\varphi)$ on the ring electrode with a high degree of symmetry. By imposing the condition

$$\frac{1}{2}\sum_{i=1}^{8} U_i \Delta_i = U_1\Delta_1 + 2U_2\Delta_2 + U_3\Delta_3 = 0 \tag{67}$$

the average of the potential is made to vanish. Let us choose the origin of the angular coordinate φ at the middle of segment 1, then we have $\varphi_1 = \Delta_1/2$, $\varphi_0 = -\Delta_1/2$, so that $\Delta_1 = \varphi_1 - \varphi_0$. Furthermore we have $\varphi_7 = 2\pi - \varphi_2$, $\varphi_6 = 2\pi - \varphi_3$, and $\varphi_5 = 2\pi - \varphi_4$. The potential function $U_{\mathrm{ell}}(\varphi)$ thus acquires the symmetry properties $U_{\mathrm{ell}}(\varphi) = U_{\mathrm{ell}}(-\varphi)$ and $U_{\mathrm{ell}}(\varphi) = U_{\mathrm{ell}}(\varphi + \pi)$. For the Fourier expansion of $U_{\mathrm{ell}}(\varphi)$ the first symmetry property implies that the Fourier series is a pure cosine series, the second property permits only terms depending on even multiples of φ. Thus for the geometry that we are here considering the Fourier expansion of the potential of the ring electrode assumes the form

$$U_{\mathrm{ell}}(\varphi) = \sum_{n=0}^{\infty} u_{2n} \cos(2n\varphi). \tag{68}$$

The condition (67) requires $u_0 = 0$. All other the Fourier components are given by

$$\begin{aligned} u_{2n} &= \frac{1}{\pi}\int_{-\pi}^{+\pi} \mathrm{d}\varphi \cdot U_{\mathrm{ell}}(\varphi)\cos(2n\varphi) \\ &= \frac{1}{n\pi}\sum_{i=1}^{4} U_i \cdot (\sin(2n\varphi_i) - \sin(2n\varphi_{i-1})) \quad (n = 1, 2, 3, \ldots) \\ &= \frac{2}{n\pi}\left[(U_1 - U_2)\cdot\sin(n\Delta_1) + (U_3 - U_2)\cdot(-1)^n \sin(n\Delta_3)\right]. \end{aligned} \tag{69}$$

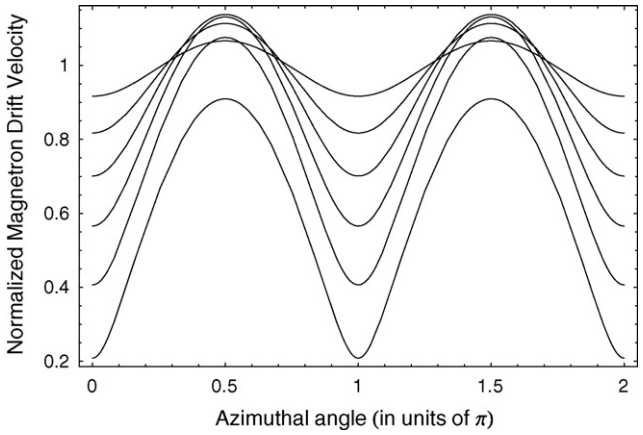

Fig. 7. Magnetron drift velocity as a function of the azimuthal angle $\tilde{\varphi}_-$ for six different values of ϵ, from top to bottom $\epsilon = 0.15, 0.3, 0.45, 0.6, 0.75$, and 0.9.

There is still freedom to define different operating modes for the segmented ring electrode: *Operating mode I*: The segments 2, 4, 6, and 8 are set on ground potential and remain unused for modeling the elliptic trap, while U_3 is fixed by the condition (67), *i.e.*, $U_2 = U_4 = U_6 = U_8 = 0$ and $U_3 = -(\Delta_1/\Delta_3)\cdot U_1$.

Operating mode II: The voltage applied to the segments 2, 4, 6, and 8 is chosen so that the Fourier coefficient u_4 vanishes, thus eliminating the leading anharmonic contribution to the potential.

Table 1
Fourier coefficients c_{2n} calculated for the segmented ring electrode of the Greifswald cluster trap, for the operating modes I and II, respectively

Operating mode I $U_2 = 0$ $U_3 = -2\,U_1$		Operating mode II $U_2 = -0.580447\,U_1$ $U_3 = -1.12933\,U_1$	
$c_2 = +1.44537$	$c_{18} = 0$	$c_2 = +1.21547$	$c_{18} = 0$
$c_4 = -0.518080$	$c_{20} = -0.0191475$	$c_4 = 0$	$c_{20} = +0.0766249$
$c_6 = +0.183776$	$c_{22} = +0.133785$	$c_6 = -0.189577$	$c_{22} = +0.0625675$
$c_8 = -0.211171$	$c_{24} = -0.137832$	$c_8 = -0.191562$	$c_{24} = -0.0978301$
$c_{10} = -0.00525245$	$c_{26} = +0.00202017$	$c_{10} = +0.105445$	$c_{26} = -0.0405557$
$c_{12} = +0.275644$	$c_{28} = +0.0603346$	$c_{12} = 0.195660$	$c_{28} = +0.0547321$
$c_{14} = -0.210233$	$c_{30} = -0.0367553$	$c_{14} = -0.0983204$	$c_{30} = +0.0379154$
$c_{16} = +0.0239343$	$c_{32} = +0.0647600$	$c_{16} = -0.0957811$	$c_{32} = 0$

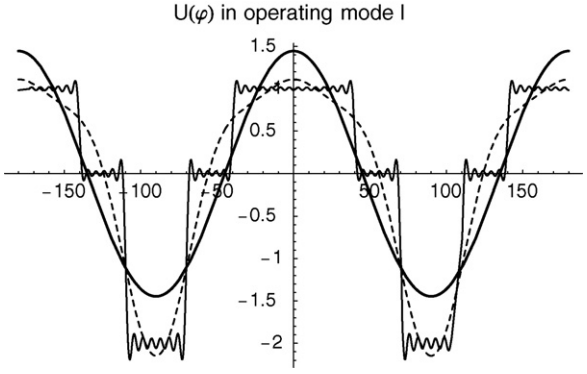

Fig. 8. Fourier decomposition of the electric potential on the ring electrode in operating mode I. The three curves show the component $\propto \cos 2\varphi$ which is taken into account by the exact solution of the ideal elliptical Penning trap (solid line), the approximation to the potential including terms $\propto \cos 2\varphi$, $\cos 4\varphi$, and $\cos 6\varphi$ (dashed line), and the representation of the potential obtained by summing the first 30 terms of the series.

Together with the condition (67)U_2 and U_3 are then determined as linear functions of U_1.

$$U_2 = U_1 \cdot \frac{\Delta_3 \sin(2\Delta_1) - \Delta_1 \sin(2\Delta_3)}{\Delta_3 \sin(2\Delta_1) + (\pi - \Delta_1)\sin(2\Delta_3)} \tag{70}$$

$$U_3 = -U_1 \cdot \frac{(\pi - \Delta_3)\sin(2\Delta_1) + \Delta_1 \sin(2\Delta_3)}{\Delta_3 \sin(2\Delta_1) + (\pi - \Delta_1)\sin(2\Delta_3)} \tag{71}$$

The Fourier expansion of $U_{\mathrm{ell}}(\varphi)$ can now be written with dimensionless coefficients $c_{2n} = u_{2n}/U_1$ as[2]

$$U_{\mathrm{ell}}(\varphi) = U_1 \sum_{n=1}^{\infty} c_{2n}^{\mu} \cdot \cos(2n\varphi) \quad (\mu = \mathrm{I}, \mathrm{II}) \tag{72}$$

As an example let us discuss the Greifswald cluster trap [12]. Here the ring electrode is divided into eight segments, with $\Delta_1 = 80^\circ$, $\Delta_2 = 30^\circ$, and $\Delta_3 = 40^\circ$. The voltages and Fourier coefficients obtained for the two operating modes are shown in Table 1. Figs. 8 and 9 illustrate for the two operating modes of the segmented ring electrode the quality of the approximation to the ideal elliptic trap. As expected, in operating mode II the elimination of the term $\propto \cos 4\varphi$ results in a better representation of the ideal case.

3.2. The electrostatic potential in the trap interior

In the preceding subsection we have analyzed the dependence on the azimuthal angle φ of the "elliptic" electrostatic potential $U_{\mathrm{ell}}(\varphi)$ on the surface of the ring electrode of the trap, in order to determine the coefficient c_2 of the component that corresponds to the ideal elliptic Penning trap. The more general problem of determining the electrostatic potential in the trap interior is important for estimates of the deformations of the ion orbits and of the shifts of the characteristic frequencies as compared to the ideal elliptic Penning trap. Already Bollen et al. [9] have demonstrated the existence of important screening effects due to the end electrodes.

The electrostatic potential in the trap interior U is sourcefree and therefore satisfies in three dimensions Laplace's differential equation. The values of the potential on the surfaces of the segmented ring electrode and the end electrodes are prescribed by the experiment, and thus a Dirichlet boundary value problem is given. As is well known its solution can be represented as an expansion in terms of spherical harmonics [11]. Using cylindrical polar coordinates r, φ,

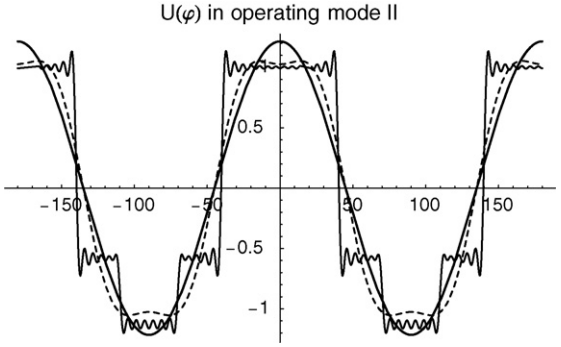

Fig. 9. Fourier decomposition of the electric potential on the ring electrode in operating mode II. The three curves show the component $\propto \cos 2\varphi$ which is taken into account by the exact solution of the ideal elliptical Penning trap (solid line), the approximation to the potential including terms $\propto \cos 2\varphi$ and $\cos 6\varphi$ (dashed line), and the representation of the potential obtained by summing the first 30 terms of the series.

[2] In the accompanying paper [5] the potential U_1 is denoted as U_{ellipt}.

and z we can write

$$U_{\mathrm{ell}}(r,\varphi,z) = \sum_{k,l} \sqrt{r^2+z^2}^{k} \cdot P_k^{\mathrm{l}}(z/\sqrt{r^2+z^2})(b_{k,l}\cos(l\varphi) + b'_{k,l}\sin(l\varphi)), \tag{73}$$

where the $P_k^{\mathrm{l}}(x)$ are associated Legendre polynomials, and where the coefficients $b_{k,l}$, $b'_{k,l}$ are to be determined by the boundary conditions. As discussed in the preceding subsection the elliptic electrostatic potential possesses the symmetry properties $U_{\mathrm{ell}}(r,\varphi,z) = U_{\mathrm{ell}}(r,-\varphi,z) = U_{\mathrm{ell}}(r,\varphi+\pi,z) = U_{\mathrm{ell}}(r,\varphi,-z)$. These imply that in the series (73) only terms $\propto \cos(l\varphi)$ occur and that k and l must be even integers: $k = 2m$ and $l = 2n$. The series expansion of the elliptical electrostatic potential can therefore be rewritten as

$$U_{\mathrm{ell}}(r,\varphi,z) = U_1 \sum_{n=1}^{\infty} c_{2n}\cos(2n\varphi) \sum_{m=0}^{\infty} a_{2n,2m} p_{2n,2m}(r,z), \tag{74}$$

where the $p_{2n,2m}(r,z)$ are homogeneous polynomials in r and z of degree $2(n+m)$, defined by

$$p_{2n,2m}(r,z) = \frac{(r^2+z^2)^{n+m} \cdot P^{2n}_{2(n+m)}(z/\sqrt{r^2+z^2})}{r_0^{2(n+m)} \cdot P^{2n}_{2(n+m)}(0)}. \tag{75}$$

The normalization of the polynomials is chosen so that on the inner radius r_0 of the ring electrode the polynomials assume the value $p_{2n,2m}(r_0,0) = 1$. The explicit form of the polynomials can be deduced from the representation of the associated Legendre polynomials in terms of hypergeometric functions [13]

$$p_{2n,2m}(r,z) = \frac{r^{2n}}{r_0^{2(n+m)}} \sum_{j=0}^{m} c_{n,m,j} r^{2(m-j)} (2z^2)^j, \tag{76}$$

with coefficients

$$c_{n,m,j} = (-1)^j \cdot \frac{\binom{m}{j}}{(2j-1)!!} \cdot \frac{(2n+m)!}{(2n+m-j)!}. \tag{77}$$

Note that $c_{n,m,0} = 1$ for all n, m. It is useful to display a few of these polynomials explicitly:

$$p_{2n,0}(r,z) = \frac{r^{2n}}{r_0^{2n}}, \tag{78}$$

$$p_{2n,2}(r,z) = \frac{r^{2n}}{r_0^{2(n+1)}} \cdot (r^2 - (2n+1)\cdot 2z^2), \tag{79}$$

$$p_{2n,4}(r,z) = \frac{r^{2n}}{r_0^{2(n+2)}} \cdot \left(r^4 - 2(2n+2)\cdot r^2 \cdot 2z^2 + \frac{1}{3}(2n+1)(2n+2)\cdot (2z^2)^2 \right), \tag{80}$$

$$p_{2n,6}(r,z) = \frac{r^{2n}}{r_0^{2(n+3)}} \cdot \left(r^6 - 3(2n+3)\cdot r^4 \cdot (2z^2)^2 + (2n+2)(2n+3)\cdot r^2 \cdot (2z^2)^2 - \frac{1}{15}(2n+1)(2n+2)(2n+3)\cdot (2z^2)^3 \right). \tag{81}$$

Finally we must discuss the coefficients $a_{2n,2m}$. The determination of all the coefficients requires a full solution of the three-dimensional boundary value problem for the elliptic electrostatic potential $U_{\mathrm{ell}}(r,\varphi,z)$, however, we shall here be content with some simple estimates.

Two obvious conditions for the coefficients $a_{n,m}$ are obtained as follows. As noted above $p_{2n,2m}(r_0,0) = 1$, therefore in the plane $z = 0$ the potential at the inner radius r_0 of the ring electrode reduces to $U_{\mathrm{ell}}(r,\varphi,z) = U_1 \sum_{n=1}^{\infty} c_{2n}\cos(2n\varphi) \sum_{m=0}^{\infty} a_{2n,2m}$, which must be identical to Eq. (72). Thus the condition

$$\sum_{m=0}^{\infty} a_{2n,2m} = 1 \quad \text{for all} \quad n = 1,2,3,\ldots \tag{82}$$

results. Similarly we use the fact that the potential U_{ell} must vanish on the end electrodes to impose at the vertices $r = 0$, $z = z_0$ the conditions

$$\sum_{m=0}^{\infty} a_{2n,2m} c_{n,m,m} \left(2z_0^2/r_0^2\right)^m = 0 \quad \text{for all} \quad n = 1,2,3,\ldots \tag{83}$$

Further approximation strategies must be devised to obtain more conditions for the $a_{2n,2m}$ and better approximations for the potential U_{ell}, however, we shall here not pursue this point any further.

The two conditions (82) and (83) are sufficient for the simplest possible estimate of the screening effects due to the end electrodes. One keeps in the expansion (74) only terms with $m = 0$ and 1, higher terms decrease with additional powers of $(r/r_0)^2$. Our two conditions reduce to the form

$$a_{2n,0} + a_{2n,2} = 1, \qquad a_{2n,0} - (2n+1)(2z_0^2/r_0^2)\cdot a_{2n,2} = 0 \quad \text{for all} \quad n = 1,2,3,\ldots \tag{84}$$

The traps used in the work by Bollen et al. [9] or in the work described in [5] are so-called "symmetric" traps with $2z_0^2 = r_0^2$. For these we obtain the solution $a_{2n,0} = (2n+1)/(2n+2)$, $a_{2n,2} = 1/(2n+2)$ for all n. For the quadrupolar terms in particular we find $a_{2,0} = 0.75$ and $a_{2,2} = 0.25$, to be compared with the results of the simulation by Bollen et al. $a_{2,0} = 0.80$ and $a_{2,2} = 0.16$. Their result is in slight violation of the conditions (82) and (83), the consequences become obvious when one plots the equipotential surfaces.

In the central plane of the trap, $z = 0$, the elliptic electrostatic potential simplifies to

$$U_{\mathrm{ell}}(r,\varphi,z)|_{z=0} = U_1 \sum_{n=1}^{\infty} c_{2n}\cos(2n\varphi) \sum_{m=0}^{\infty} a_{2n,2m} (r/r_0)^{2(n+m)}. \tag{85}$$

We can identify here the term defining the ideal elliptic Penning trap

$$qU_1 \cdot c_2^{\mu} \cdot a_{2,0} \cdot \left(\frac{r}{r_0}\right)^2 \cos(2\varphi) = \kappa \cdot \frac{m\omega_1}{2} \cdot r^2 \cos(2\varphi) = \frac{qU_0}{2z_0^2 + r_0^2} \cdot \epsilon \cdot r^2 \cos(2\varphi), \tag{86}$$

whence we can relate the ellipticity parameters ϵ and κ to the applied voltage U_1

$$\epsilon = \frac{2z_0^2 + r_0^2}{r_0^2} \cdot \frac{U_1}{U_0} \cdot c_2^{\mu} \cdot a_{2,0}, \qquad \kappa = \frac{2qU_1 \cdot u_2^{\mu} \cdot a_{2,0}}{m\omega_1 r_0^2}. \tag{87}$$

Fig. 10 shows the equipotential lines for the circular and the ideal elliptic Penning trap together with those for the sum of the anharmonic perturbation terms and those for the perturbed elliptic trap. With increasing distance from the trap center the deformation of the ellipses due to anharmonic terms becomes quite notable. This fact is of interest because the magnetron drift of the ions in

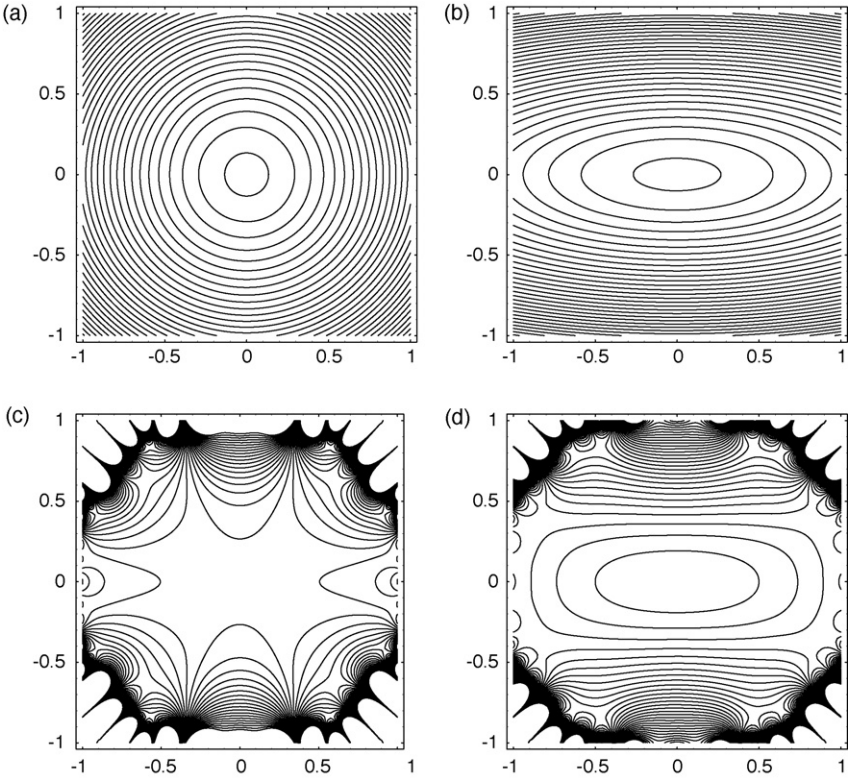

Fig. 10. Equipotential lines for (a) the ideal circular Penning trap, (b) the ideal elliptical Penning trap, (c) the anharmonic perturbations due to the segmented ring electrode in operating mode I, and (d) the elliptical Penning trap including anharmonic terms. The calculation assumed the operational mode I and an ellipticity parameter $\epsilon = 0.75$.

the trap follows roughly the equipotential lines. These figures may be compared with the results obtained by numerical simulations of the equipotential lines and the ion orbits as described in the accompanying experimental investigation [5].

3.3. Results of perturbation theory

The deviations of the electric potential of a real elliptical Penning trap from that of an ideal trap cause distortions of the ion orbits and shifts of the characteristic frequencies. These can be estimated by use of canonical classical perturbation theory [7,8]. It may be helpful to sketch the basic idea of this method, which is formulated in terms of action and angle variables and uses the Hamiltonian of the ideal elliptical Penning trap (28) as its starting point. The angle variables are the phases $\tilde{\varphi}_\pm(t) = \tilde{\omega}_\pm t + \tilde{\chi}_\pm$, the canonically conjugate action variables are obtained by

$$\tilde{J}_+ = \frac{1}{2\pi}\oint \tilde{p}_+ \mathrm{d}\tilde{q}_+ = \frac{\tilde{A}_+^2}{2}, \tag{88}$$

$$\tilde{J}_- = \frac{1}{2\pi}\oint \tilde{p}_- \mathrm{d}\tilde{q}_- = -\frac{\tilde{A}_-^2}{2}. \tag{89}$$

In these variables Eq. (28) assumes the form

$$\tilde{H}(\tilde{q},\tilde{p}) = \tilde{H}(\tilde{\varphi}_+,\tilde{\varphi}_-,\tilde{J}_+,\tilde{J}_-) = \tilde{\omega}_+\tilde{J}_+ + \tilde{\omega}_-\tilde{J}_-. \tag{90}$$

Obviously $\tilde{\omega}_\pm = \mathrm{d}\tilde{\varphi}_\pm/\mathrm{d}t = \partial\tilde{H}/\partial\tilde{J}_\pm$. We also note that the action variables $\tilde{J}_\pm$ are related to the size parameters $\tilde{R}_\pm$ by

$$\tilde{J}_+ = \frac{1}{2}m\omega_1\tilde{R}_+^2, \qquad \tilde{J}_- = -\frac{1}{2}m\omega_1\tilde{R}_-^2. \tag{91}$$

The Hamiltonian of the real elliptic Penning trap is then constructed by adding the perturbing potential V_1 (to be specified below) to $\tilde{H}$ and by transforming this new Hamiltonian $\hat{H}$ to a new set of action and angle variables $\hat{J}_\pm$, $\hat{\varphi}_\pm$ with the property that $\hat{H}$ is independent of the new angle variables and is only a function of the new action variables, in other words, the new angle variables $\hat{\varphi}_\pm$ are again cyclic coordinates, while the new action variables $\hat{J}_\pm$ are constants of the motion.

$$\tilde{H}(\tilde{\varphi}_+,\tilde{\varphi}_-,\tilde{J}_+,\tilde{J}_-) + \tilde{V}_1(\tilde{\varphi}_+,\tilde{\varphi}_-,\tilde{J}_+,\tilde{J}_-) = \hat{H}(\hat{J}_+,\hat{J}_-). \tag{92}$$

Hamilton's equations of motion now yield the perturbed characteristic frequencies, $\hat{\omega}_\pm = \mathrm{d}\hat{\varphi}_\pm/\mathrm{d}t = \partial\hat{H}/\partial\hat{J}_\pm$, and the constancy of the action variables, $\mathrm{d}\hat{J}_\pm/\mathrm{d}t = -\partial\hat{H}/\partial\hat{\varphi} = 0$. The former variables $\tilde{\varphi}_\pm(t)$, $\tilde{J}_\pm$ are related to the new variables $\hat{\varphi}_\pm$, $\hat{J}_\pm$ by a canonical transformation with the generator

$$S(\tilde{\varphi}_+,\tilde{\varphi}_-,\hat{J}_+,\hat{J}_-) = \tilde{\varphi}_+\hat{J}_+ + \tilde{\varphi}_-\hat{J}_- + S_1(\tilde{\varphi}_+,\tilde{\varphi}_-,\hat{J}_+,\hat{J}_-), \tag{93}$$

implying

$$\hat{\varphi}_\pm = \frac{\partial S}{\partial\hat{J}_\pm} = \tilde{\varphi}_\pm + \frac{\partial S_1}{\partial\hat{J}_\pm} \qquad \tilde{J}_\pm = \frac{\partial S}{\partial\tilde{\varphi}_\pm} = \hat{J}_\pm + \frac{\partial S_1}{\partial\tilde{\varphi}_\pm}. \tag{94}$$

Canonical perturbation theory essentially consists of a systematic procedure for the determination of the generator function $S_1(\tilde{\varphi},\hat{J})$. The construction is somewhat involved, we therefore refer for details to the literature [7,8]. In this paper we focus our attention on the simplest, but most important term in the perturbation series, which can be obtained according to the following recipe: expand $\tilde{V}_1(\tilde{\varphi}_+,\tilde{\varphi}_-,\tilde{J}_+,\tilde{J}_-)$ into a multiple Fourier series with respect to the angle variables $\tilde{\varphi}_+$, $\tilde{\varphi}_-$, select the constant term, *i.e.*, the one independent of $\tilde{\varphi}_\pm$, and substitute $\hat{J}_\pm$ in place of $\tilde{J}_\pm$. In other words, calculate

$$V_1^{(00)}(\hat{J}_+,\hat{J}_-) = \frac{1}{(2\pi)^2}\int_{-\pi}^{+\pi}\mathrm{d}\varphi_+\int_{-\pi}^{+\pi}\mathrm{d}\varphi_-\tilde{V}_1(\tilde{\varphi}_+,\tilde{\varphi}_-,\tilde{J}_+,\tilde{J}_-), \tag{95}$$

substitute $\tilde{J}_\pm \to \hat{J}_\pm$, and write

$$\hat{H}(\hat{J}_+,\hat{J}_-) \approx \hat{\omega}_+\hat{J}_+ + \hat{\omega}_-\hat{J}_- + V_1^{(00)}(\hat{J}_+,\hat{J}_-). \tag{96}$$

Hamilton's equations of motion yield the perturbed frequencies and the conservation of the actions

$$\hat{\omega}_\pm = \frac{\mathrm{d}}{\mathrm{d}t}\hat{\varphi}_\pm = \frac{\partial}{\partial \hat{J}_\pm}\hat{H}(\hat{J}_+,\hat{J}_-) \qquad \frac{\mathrm{d}}{\mathrm{d}t}\hat{J}_\pm = -\frac{\partial}{\partial \hat{\varphi}_\pm}\hat{H}(\hat{J}_+,\hat{J}_-) = 0. \tag{97}$$

Finally the desired information about the frequency shifts due to the additional potential $\tilde{V}_1(\tilde{\varphi}_+,\tilde{\varphi}_-,\tilde{J}_+,\tilde{J}_-)$ is obtained as

$$\Delta\tilde{\omega}_\pm = \hat{\omega}_\pm - \tilde{\omega}_\pm \approx \frac{\partial}{\partial \hat{J}_\pm} V_1^{(00)}(\hat{J}_+,\hat{J}_-). \tag{98}$$

3.3.1. Frequency shifts due to anharmonic terms in the trap potential

In Section 3.2 we have considered the potentials applied to the segments of the ring electrode and have investigated what we can learn about the potential in the trap interior. For the central plane of the trap, $z = 0$, we found the representation Eq. (85). Here we use this potential to calculate by means of canonical perturbation theory the shifts of the magnetron and modified cyclotron frequencies caused by the anharmonic terms. Following the recipe developed above we have to transform the potential (85) to the action and angle variables of the ideal elliptical trap, for which we know the exact solutions of the equations of motion and which serves as the 0-th approximation in the perturbation approach. To be more specific, we have to express the polar coordinates $r(t)$, $\varphi(t)$ in terms of the phase angles $\tilde{\varphi}_+(t)$, $\tilde{\varphi}_-(t)$ and the actions $\tilde{J}_+(t)$,$\tilde{J}_-(t)$. As starting point we use Eqs. (57), (58) and (91) to write

$$\begin{aligned} r(t)\exp[+i\varphi(t)] &= x(t) + iy(t) = (x_+(t) + x_-(t)) + i(y_+(t) + y_-(t)) \\ &= \frac{1}{\sqrt{m\omega_1}}[\xi_+\tilde{q}_+(t) + \xi_-\tilde{q}_-(t)] + \frac{i}{\sqrt{m\omega_1}}[\eta_+\tilde{p}_+(t) \\ &\quad -\eta_-\tilde{p}_-(t)] = \sqrt{\frac{2\tilde{J}_+}{m\omega_1}}[\xi_+\cos\tilde{\varphi}_+(t) \\ &\quad -i\eta_+\sin\tilde{\varphi}_+(t)] \\ &\quad +\sqrt{\frac{-2\tilde{J}_-}{m\omega_1}}[\xi_-\cos\tilde{\varphi}_-(t) - i\eta_-\sin\tilde{\varphi}_-(t)]. \end{aligned} \tag{99}$$

This result enables us to express $r^2 = (x+iy)(x-iy)$ and $r^{2n}\cos(2n\varphi) = (1/2)[(x+iy)^{2n} + (x-iy)^{2n}]$ in terms of canonical action and angle variables. After insertion of the results into Eq. (85), the potential must be written as a multiple Fourier series and the constant term, *i.e.*, the one independent of the phase angles $\tilde{\varphi}_\pm$, must be determined. As is evident the general case leads to very complicated expressions. We therefore content ourselves with discussing the cases of pure magnetron motion ($\tilde{J}_+ = 0, \tilde{J}_- \neq 0$) or pure modified cyclotron motion ($\tilde{J}_+ \neq 0, \tilde{J}_- = 0$). For example, in these cases $r^2(t)$ reduces to

$$r^2(t) = \pm\frac{2\tilde{J}_\pm}{m\omega_1}\cdot\left(\frac{1}{2}(\xi_\pm^2+\eta_\pm^2) + \frac{1}{2}(\xi_\pm^2-\eta_\pm^2)\cos 2\tilde{\varphi}_\pm(t)\right), \tag{100}$$

and the perturbation term in Eq. (96) simplifies to

$$\begin{aligned} V_1^{(0)}(\tilde{J}_\pm) &= qU_1\cdot\sum_{n=2}^{\infty}(\pm1)^n c_{2n}\cdot a_{2n,0}\left(\frac{2\tilde{J}_\pm}{m\omega_1 r_0^2}\right)^n\cdot\frac{1}{2^n}\begin{pmatrix}2n\\n\end{pmatrix} \\ &\quad\times\left[\frac{1}{2}\left(\xi_\pm^2-\eta_\pm^2\right)\right]^n + qU_1\cdot\sum_{n=2}^{\infty}(\pm1)^{n+1}c_{2n}\cdot a_{2n,2} \\ &\quad\times\left(\frac{2\tilde{J}_\pm}{m\omega_1 r_0^2}\right)^{n+1}\cdot\frac{1}{2^n}\left[\begin{pmatrix}2n\\n\end{pmatrix} + \begin{pmatrix}2n\\n-1\end{pmatrix}\right] \\ &\quad\times\left[\frac{1}{2}\left(\xi_\pm^2-\eta_\pm^2\right)\right]^n\cdot\left[\frac{1}{2}\left(\xi_\pm^2+\eta_\pm^2\right)\right]. \end{aligned} \tag{101}$$

Finally we substitute $\tilde{J}_\pm \to \hat{J}_\pm$ and apply Eqs. (96)–(98) to obtain the desired frequency shift

$$\begin{aligned} \Delta\tilde{\omega}_\pm &= \hat{\omega}_\pm - \tilde{\omega}_\pm = \frac{\partial V_1^{(0)}(\hat{J}_\pm)}{\partial \hat{J}_\pm} \\ &= \pm\frac{2qU_1}{m\omega_1 r_0^2}\sum_{n=2}^{\infty}c_{2n}\cdot a_{2n,0}\cdot\frac{(2n-1)!!}{(n-1)!}\cdot\left(\frac{\tilde{R}_\pm}{r_0}\right)^{2(n-1)} \\ &\quad\times\left[\frac{1}{2}(\xi_\pm^2-\eta_\pm^2)\right]^n \pm\frac{2qU_1}{m\omega_1 r_0^2}\sum_{n=2}^{\infty}c_{2n}\cdot a_{2n,2}\cdot\frac{(2n+1)!!}{n!} \\ &\quad\times\left(\frac{\tilde{R}_\pm}{r_0}\right)^{2n}\cdot\left[\frac{1}{2}(\xi_\pm^2-\eta_\pm^2)\right]^n\cdot\left[\frac{1}{2}(\xi_\pm^2+\eta_\pm^2)\right]. \end{aligned} \tag{102}$$

The Fourier coefficients c_{2n} have been determined by Eq. (72), for the coefficients $a_{2n,0}$ and $a_{2n,2}$ we use our previous estimates $a_{2n,0} = (2n+1)/(2n+2)$, $a_{2n,2} = 1/(2n+2)$. For a comparison of this theoretical prediction with experimental data see the accompanying article [5].

3.3.2. Frequency shifts due to image charges

Each ion in the trap induces image charges on the electrode surfaces, the image charges in turn exert an attractive force on the ion and thus shift the characteristic frequencies of the ion orbit. For hyperbolic surfaces image charges are difficult to calculate in general. van Dyck et al. [14] therefore suggested that for ion orbits in the equatorial plane $z = 0$ a good approximation might be obtained by considering instead of the hyperbolic electrode surfaces a conducting sphere with a radius r_0 equal to the inner radius of the ring electrode. For a spherical surface the calculation of the image charge distribution is elementary [11]. It leads to the result that the image charges induced by a cloud of N ions with its center at $\mathbf{r} = x\mathbf{e}_x + y\mathbf{e}_y$ exert a force on each single ion which is given by [14]

$$\mathbf{F} = \frac{Nq^2r_0\cdot\mathbf{r}}{(r_0^2-r^2)^2} = -\frac{\mathrm{d}}{\mathrm{d}r}V_{\mathrm{image}}(r) \tag{103}$$

where $r = |\mathbf{r}|$ and

$$V_{\mathrm{image}}(r) = -\frac{Nq^2r_0}{2(r_0^2-r^2)} = -\frac{Nq^2}{2r_0}\left(1 + \frac{r^2}{r_0^2} + \sum_{j=2}^{\infty}\frac{r^{2j}}{r_0^{2j}}\right). \tag{104}$$

is the potential of this force. In the series expansion of the potential the constant first term is irrelevant, while the second term $\propto r^2$ can be combined with the Hamiltonian (5) for a redefinition of the frequencies ω_1, ω_+, and ω_-. It thus leads to an overall frequency shift $\Delta\omega_\pm \approx \mp(Nq^2/(m\omega_1 r_0^3))$ independent of the orbital parameters of the ions. The remaining terms in (104) are anharmonic and shall in the following be studied by perturbation theory.

Let us now calculate for the elliptical Penning trap the shifts of the cyclotron and magnetron frequencies due to image charges. Again the first step is the transformation of the additional potential V_{image} in Eq. (104) to the action and angle variables of the elliptic trap, *i.e.*, to $\tilde{J}_\pm$ and $\tilde{\varphi}_\pm$, using the substitutions described in the preceding subsection. The general case is quite involved. Considerable simplifications take place for pure cyclotron motion ($\tilde{J}_+ \neq 0$, $\tilde{J}_- = 0$) and for pure magnetron motion ($\tilde{J}_+ = 0$, $\tilde{J}_- \neq 0$). After insertion of

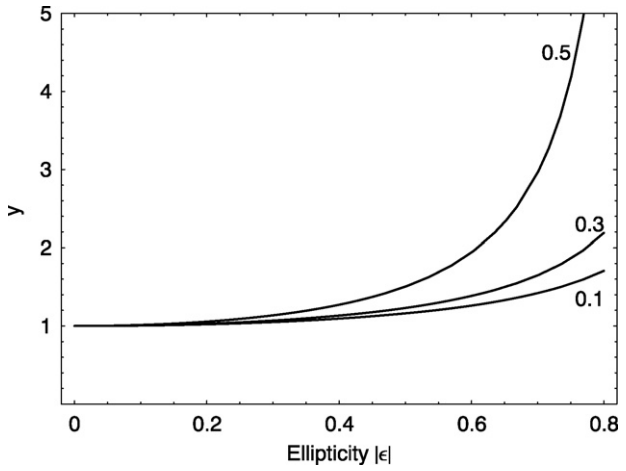

Fig. 11. Magnetron frequency shift due to image charges as a function of the ellipticity $|\epsilon|$. The plot shows the ratio of the magnetron frequency shift in the elliptical trap to the magnetron frequency shift in the corresponding circular trap ($\epsilon = 0$), *i.e.*, $y = \Delta\tilde{\omega}_-(\epsilon)/\Delta\omega_-$, for three different orbit sizes, $\tilde{R}_-/r_0 = 0.1$, 0.3, and 0.5.

expression (100) into Eq. (104) the potential $V_{\text{image}}(r)$ can be considered as a Fourier series with respect to the angle variable $\tilde{\varphi}_\pm$. Its constant term, *i.e.*, the one independent of $\tilde{\varphi}_\pm$, considered as a function of $\tilde{J}_\pm$, yields the leading contribution to the perturbation theoretic result. This term is most easily obtained according to the rule for calculating Fourier coefficients, namely by the integral

$$V^0_{\text{image}}(\tilde{J}_\pm) = \frac{1}{2\pi}\int_{-\pi}^{+\pi} \mathrm{d}\tilde{\varphi}_\pm V_{\text{image}}(\tilde{\varphi}_\pm) \tag{105}$$

$$= -\frac{Nq^2}{2r_0}\cdot\left(1+\frac{2\tilde{J}_\pm}{m\omega_1 r_0^2}\cdot\xi_\pm^2\right)^{-1/2}\left(1+\frac{2\tilde{J}_\pm}{m\omega_1 r_0^2}\cdot\eta_\pm^2\right)^{-1/2} \tag{106}$$

After the substitution of $\tilde{J}_\pm \to \hat{J}_\pm$ we now obtain the frequency shift due to image charges from Eq. (98)

$$\frac{\partial\hat{H}}{\partial\hat{J}_\pm} = \hat{\omega}_\pm = \tilde{\omega}_\pm + \frac{\partial V^{(0)}_{\text{image}}(\hat{J}_\pm)}{\partial\hat{J}_\pm}. \tag{107}$$

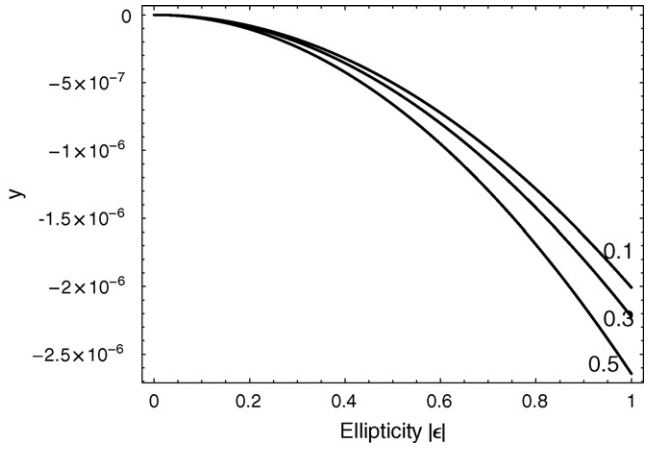

Fig. 12. Cyclotron frequency shift due to image charges as a function of the ellipticity $\epsilon = \kappa/\kappa_{\max}$. The plot shows the deviation from 1 of the ratio of the cyclotron frequency shift in the elliptical trap to the cyclotron frequency shift in the corresponding circular trap ($\epsilon = 0$), *i.e.*, $y = (\Delta\tilde{\omega}_+(\epsilon)/\Delta\omega_+) - 1$, for three different orbit sizes, $\tilde{R}_+/r_0 = 0.1$, 0.3, and 0.5.

The result is

$$\Delta\tilde{\omega}_- = \hat{\omega}_- - \tilde{\omega}_- = \frac{Nq^2}{2m\omega_1 r_0^3}\cdot\frac{\xi_-^2+\eta_-^2-2(\tilde{R}_-^2/r_0^2)\xi_-^2\eta_-^2}{[(1-(\tilde{R}_-^2/r_0^2)\xi_-^2)(1-(\tilde{R}_-^2/r_0^2)\eta_-^2)]^{3/2}}. \tag{108}$$

The dependence on the ellipticity parameter ϵ is contained in the expressions for the normalized semi-axes ξ_- and η_-. (The geometrical semi-axes are $\xi_-\tilde{R}_-$ and $\eta_-\tilde{R}_-$.) In the limit $\epsilon \to \pm 1$ the expression diverges due to the growth of the major semi-axis of the magnetron orbit. On the other end, in the limit $\epsilon \to 0$ we have $\xi_- \to 1$ and $\eta_- \to 1$. The magnetron orbit becomes circular with radius $R_- = \tilde{R}_-$. The expression for the frequency shift reduces to

$$\Delta\omega_- = \frac{Nq^2 r_0}{m\omega_1}\cdot\frac{1}{(r_0^2-R_-^2)^2}, \tag{109}$$

in agreement with the result obtained by Vogel et al. [15] for circular Penning traps. In Fig. 11 we have plotted as a function of the ellipticity ϵ the ratio of the frequency shifts due to image charges expected for the elliptical trap and the circular trap. Analogous formulas are obtained for the modified cyclotron frequency, however, numerically the corrections are much smaller. Therefore we have plotted in Fig. 12 only the deviation from 1 of the ratio of the frequency shifts expected for the elliptical and the circular trap.

$$\Delta\tilde{\omega}_+ = \hat{\omega}_+ - \tilde{\omega}_+ = -\frac{Nq^2}{2m\omega_1 r_0^3}\cdot\frac{\xi_+^2+\eta_+^2-2(\tilde{R}_+^2/r_0^2)\xi_+^2\eta_+^2}{[(1-(\tilde{R}_+^2/r_0^2)\xi_+^2)(1-(\tilde{R}_+^2/r_0^2)\eta_+^2)]^{3/2}} \tag{110}$$

4. Conclusions

The conventional hyperbolical Penning trap with cylindrical symmetry has been generalized to a field configuration with elliptical geometry by introducing an additional static electric quadrupolar potential $\propto \epsilon(x^2-y^2)$, where ϵ is a strength parameter called "ellipticity". In the ideal case the ion motion is governed by a Hamiltonian which is quadratic in coordinates and canonical momenta, consequently the equations of motion are linear and can be rigorously solved. The dynamics of the ion motion has been completely analyzed and described in detail. For realistic values of the trap parameters the cyclotron motion is only slightly affected, however, with increasing $|\epsilon|$ the magnetron orbit becomes more and more elliptic and degenerates into a straight line for $|\epsilon| = 1$. For even stronger quadrupolar fields the magnetron drift motion changes its character from a bounded elliptic motion into an unbounded hyperbolic motion. One of the most interesting aspects of an elliptical trap is the fact that with increasing $|\epsilon|$ the magnetron frequency decreases, until it vanishes for $|\epsilon| = 1$. The drift velocity is no longer constant, but varies along the orbit.

In practice the "elliptical" Penning trap is realized by use of a ring electrode divided into four or eight segments to approximately generate a static quadrupolar potential. Unavoidably higher multipoles are generated as well and make their influence felt on the ion motion in regions far from the trap center. These anharmonic terms have been studied in some detail, in particular screening effects due to the end electrodes and the induced potential due to image charges of the ions have been discussed. Shifts of the characteristic frequencies due to these anharmonic terms have been estimated by classical canonical perturbation theory, in support of the concurrent experimental investigation by Breitenfeldt et al. [5].

References

[1] L.S. Brown, G. Gabrielse, Rev. Mod. Phys. (1986) 233.
[2] K. Pradip Gosh, Ion Traps, Clarendon Press, Oxford, 1995.
[3] F.G. Major, V.N. Gheorghe, G. Werth, Charged Particle Traps, Springer-Verlag, Berlin Heidelberg, New York, 2005.
[4] K. Blaum, Phys. Rep. 425 (2006) 1.
[5] M. Breitenfeldt, S. Baruah, K. Blaum, A. Herlert, M. Kretzschmar, F. Martinez, G. Marx, L. Schweikhard, N. Walsh, Int. J. Mass Spectrom. (2008) this issue.
[6] L.S. Brown, G. Gabrielse, Phys. Rev. A 25 (1982) 2423.
[7] M. Kretzschmar, Z. Naturforsch. 45a (1990) 965.
[8] M. Kretzschmar, Phys. Scr. 46 (1992) 544.
[9] G. Bollen, R.B. Moore, G. Savard, H. Stolzenberg, J. Appl. Phys. 68 (1990) 4355.
[10] M. Kretzschmar, Eur. J. Phys. 12 (1991) 240.
[11] J.D. Jackson, Classical Electrodynamics, 2nd ed., John Wiley & Sons, New York, 1975.
[12] L. Schweikhard, S. Krückeberg, K. Lützenkirchen, C. Walther, Eur. Phys. J. D 9 (1999) 15.
[13] I.S. Gradshteyn, I.M. Ryzhik, Table of Integrals, Series, and Products, Academic Press, New York/London, 1965, no. 8.812 on p. 1015.
[14] R.S. van Dyck, F.L. Moore, D.L. Farnham, P.B. Schwinberg Jr., Phys. Rev. 40 A (1989) 6308.
[15] M. Vogel, H.-J. Kluge, L. Schweikhard, The Ohio State University ICR/Ion Trap Newsletter No. 21, 35 (1991).